Numerical validation of experimental temperature evolution in photovoltaic cells with varying ambient conditions

J. Sarwar [1,*], S. McCormack [2], M.J. Huang [3], B. Norton[1]
[1] Dublin Energy Lab, Dublin Institute of Technology, Kevin Street, Dublin 8, Ireland
[2] Department of Civil, Structural & Environment Engineering, Trinity College Dublin, Dublin 2, Ireland.
[3] Centre for Sustainable Technologies, School of the Built Environment, University of Ulster, Newtownabbey, Co. Antrim, BT37 0QB, UK
[*]Corresponding Author

Abstract

Photovoltaic (PV) converts solar energy to electrical energy. Part of the absorbed solar energy generates electricity but a greater proportion is converted into heat which gives rise to operating temperature of PV. Change in temperature evolution at constant insolation but varying ambient conditions were investigated in this paper along with the resultant power output. Temperature evolution in PV at insolation level of 1000Wm^{-2} was simulated using Ritz-Galerkin method in MATLAB. Two-dimensional heat conduction equation was used along with equations for natural convection and radiation losses for simulating temperature evolution in PV. Simulated results were compared with indoor experimental results at an ambient temperature of 25^{o}C validating the model. Ambient temperature was varied from 25 ^{o}C to 45 ^{o}C in steps of 10 ^{o}C. Temperature evolution and power output at each ambient condition were simulated to analyse the effect of ambient temperature. Increase in the temperature of PV was observed with the increase in the ambient temperature at constant insolation and the resultant drop in power is quantified.

Introduction

Photovoltaic (PV) converts solar energy to electrical energy. Part of the absorbed solar energy generates electricity and a greater proportion converted into heat which increaser operating temperature[1]. Crystalline silicon PV, operating above 25ºC typically, shows a temperature-dependent power decrease between 0.4%/K to 0.65%/K [2] The cell generates more power with the increase in irradiance. Irradiance has a large effect on short-circuit current while the effect on open-circuit voltage is weak. But increase in temperature results in drop of voltage at high voltages thereby reducing the power output [3]. Ambient temperature also effect the output power of PV and usually falls at a rate of ~0.5%/ ^{o}C [4]. The finite element method is a suitable computational technique for simulating temperature evolution in PV. It provides the solution of differential and integral equations which is a generalization of the classical Variational (i.e. the Ritz) and weighted-residual (e.g. Galerkin) methods [5, 6].

Experimental Setup

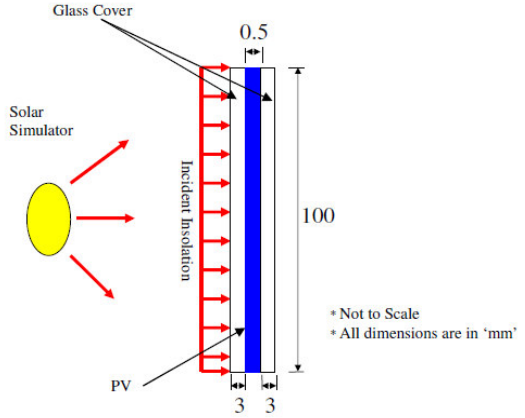

Figure 1: Experimental setup and dimensions[*]

Figure 1 shows the schematic diagram of the experimental setup and its dimensions. Five thermocouples were attached to the front and three thermocouples were attached to the back surface of the PV to record the temperature evolution on the PV at simulated insolations of 1000Wm^{-2} in indoor conditions at an ambient temperature varying in the range of 20^{o}C to 25^{o}C.

Modelled Heat Transfer Mechanism

Heat loss due to conduction, convection and radiation was considered. The schematic diagram of heat transfer mechanism in PV is shown in figure 2. Differential equation governing transient heat transfer in two dimensions is given as:

$$\rho c \frac{\partial T}{\partial t} - \left[\frac{\partial}{\partial x_i} \left(k_{ij} \frac{\partial T}{\partial x_j} \right) \right] = 0 \qquad (1)$$

Boundary flux (Incident irradiance) at the boundary is given as 'q'. Convection and radiation heat losses are considered at boundary given by following equations [7]:

$$q_c = h_c A \left(T - T_a \right) \qquad (2)$$

$$q_r = h_r A(T - T_a) \quad (3)$$

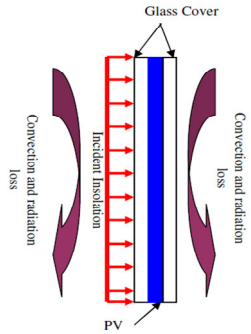

Figure 2: Heat Transfer Mechanism in PV.

Convective heat transfer coefficient is calculated as follows:

$$h_c = \frac{Nu * k}{L} \quad (4)$$

Average Nusselt number correlation for laminar flow on a flat plate is calculated as[8]:

$$Nu = 0.68 + 0.670(Ra\psi)^{\frac{1}{4}} \text{ for } Ra \le 10^9 \quad (5)$$

And for turbulent flow,

$$Nu = 0.68 + 0.670(Ra\psi)^{\frac{1}{4}}\left(1 + 1.6\times10^{-8} Ra\psi\right)^{\frac{1}{12}} \text{ for}$$

$$10^9 \le Ra < 10^{12} \text{ and } \psi = \left[1 + \left(\frac{0.492}{\Pr}\right)^{\frac{9}{16}}\right]^{-\frac{16}{9}} \quad (6)$$

Rayleigh number (Ra) is a function of Grasshoff number and Prandtl number and given as[7]:

$$Ra = Gr\Pr \text{ where } Gr = \beta\Delta T g L^3 / v^2 \quad (7)$$

Radiative heat transfer coefficient is calculated as follows[7]:

$$h_r = \sigma\varepsilon F\left(\frac{T^4 - T_a^4}{T - T_a}\right) \quad (8)$$

Element matrices

Weak formulation (Ritz-Galerkin model)[5, 9, 10] of the governing equations and boundary conditions are generated using temperature as primary variable. Bilinear LAGRANGIAN quadrangular element is used as interpolation functions for approximating element matrices of conduction, convection, radiation, mass and boundary conditions. Approximated Element matrices of conduction (K), convection (H), mass (M), radiation (R) and boundary flux (q) are given in equations 9 to 13 respectively.

$$K = \int_{-1}^{1}\int_{-1}^{1} B^T kB\left|J\right| w\partial\xi_1\partial\xi_2 \quad (9)$$

$$H = \int_{-1}^{1} N^T N h_c \left|J_i\left(\xi_1^*, \xi_2^*\right)\right| w\partial\xi_{1*or2*} \quad (10)$$

$$i = 1,..4$$

$$M = \int_{-1}^{1}\int_{-1}^{1} N^T N\rho\left|J\right| w\partial\xi_1\partial\xi_2 \quad (11)$$

$$R = \int_{-1}^{1} N^T N h_r \left|J_i\left(\xi_1^*, \xi_2^*\right)\right| w\partial\xi_{1*or2*} \quad (12)$$

$$i = 1,..4$$

$$q_f^4 = \int_{-1}^{1} N^T N\frac{q}{2}\left|J_i\left(\xi_1^*, \xi_2^*\right)\right| h\partial\xi_{1*or2*} \quad (13)$$

$$i = 1,..4$$

Numerical integration

To solve the integral expressions of element matrices presented in equations 10-14, numerical integration is applied as analytical integration is very demanding or not at all possible for the entire shape diversity of an element type [10]. 2-D numerical Gauss Legendre integration is used with n^2 gauss points to accurately analyse a bipolynomial degree $p = 2n - 1$. [11]

Mesh Generation and Assembly

Mesh is generated by subdividing the physical domain into finite elements using bilinear LAGRANGIAN element to approximate the geometry of the domain. Local node numbering stays the same for all the elements because that determines the position of coefficients in element matrices of conduction, convection, radiation, mass and boundary flux. Global node numbers are generated keeping "semi-bandwidth" minimum[9]. The assembly of elements was realized using direct addition of components[10] and only non-zero coefficients of system matrix was stored in one dimensional array[12, 13].
Crank-Nicholson finite difference scheme was used for temporal discretization and solution as it is second order accurate and stable[14].

Electrical Output Model

For the simulation of electrical output of the PV module, it is assumed that single cell voltage is equal to module voltage divided by the number of cells in series as it can be complex task to relate $I - V$ curve of a cell with the whole module.

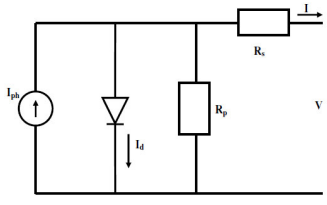

Figure 3: Equivalent circuit for PV cell

Therefore, the current 'I'can be written as classical single diode model of a PV cell as shown in figure 3[15]:

$$I = I_{ph} - I_o\left[\exp\left\{\frac{V + I.R_s}{n.V_T}\right\} - 1\right] - \frac{V + I.R_s}{R_p} \qquad (14)$$

Where I_o is the reverse saturation diode current, I_{ph} is the photo generated current, n is the ideality factor >1; V is the mean cell voltage, R_s and R_p are the series and parallel resistances. V_T is the thermal voltage and defined as:

$$V_T = BT/e \qquad (15)$$

Where'B'is Boltzmann's constant,'T'is temperature and 'e'is the electron charge. I_{ph} is described as proportional to incidence irradiance 'q'; [15]

$$I_{ph} = q.\left(C_{PT}.T + C_{PG}\right) \qquad (16)$$

The reverse saturation diode current is dependent on temperature and can be written in following form:

$$I_d = C_d T^3 \exp\left\{\frac{eV_{gap}}{B.T}\right\} \qquad (17)$$

V_{gap} is the band-gap voltage and C_d is the constant.

The Downhill-simplex method was used to find the parameter C_{PT}, C_{PG}, C_d, n, R_p and R_s to best represent the real system. The Newton-Raphson scheme was used then to numerically solve equation 14.

Results and Discussions

Figure 4 shows both experimental and simulated temperature evolution on front of PV at insolation of 1000Wm^{-2}.

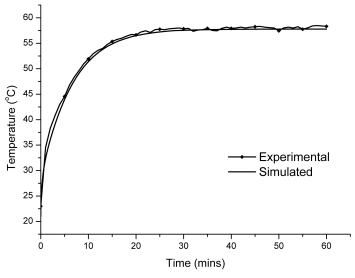

Figure 4: Experimental and Simulated temperature evolution at 1000Wm^{-2}

The initial ambient temperature during experiment was 20 °C and it rises to 23°C and simulated ambient temperature was 23 °C. The initial gradient of temperature evolution during experiment was higher than simulated results but as ambient temperature coincides, the gradient of both curves were in good agreement. The maximum temperature at 1000Wm^{-2} was ~57 °C in 30 minutes.

Figure 5 shows simulated temperature evolution at 1000Wm^{-2} with varying ambient temperature of 25°C, 35°C and 45 °C. The maximum temperature was 59.7 °C, 69.2 °C and 78.6 °C respectively. Thus increase in ambient temperature at constant irradiance results in increase in temperature of PV.

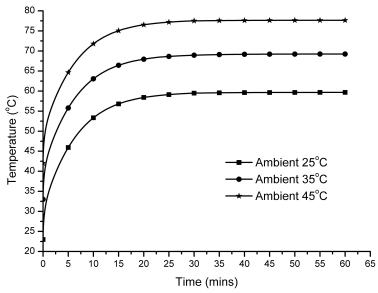

Figure 5: Simulated temperature evolution at 1000Wm^{-2} with varying ambient temperature

The linear increase in maximum temperature of the cell with the increase in ambient temperature was observed at constant irradiance during simulation and is shown in figure 6.

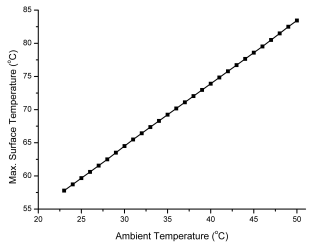

Figure 6: Temperature evolution at 1000Wm^{-2} with varying ambient temperature

The I-V curves and drop in power as a result of increased cell temperature at constant irradiance of 1000Wm^{-2} but varying ambient temperature were investigated and results are shown in figure 7 and 8.

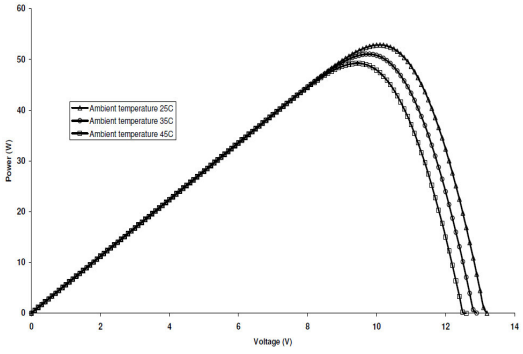

Figure 7: Power curve at 1000Wm^{-2} with varying ambient temperature

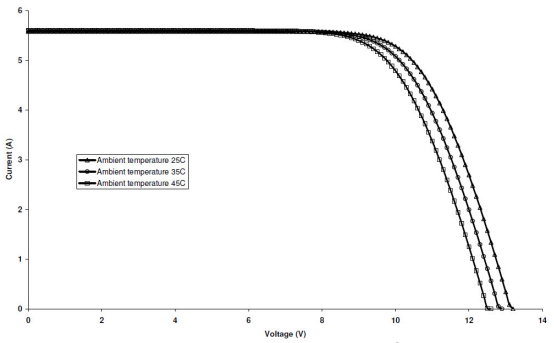

Figure 8: I-V curve at 1000Wm^{-2} with varying ambient temperature

The power drop of ~0.36%/ ^{o}C was observed with the increase in ambient temperature which was consistent with earlier investigations[4]. As irradiance was kept constant so variation in short circuit current was small as it depends less on cell temperature. But Increase in temperature results in drop of voltage at high voltages thereby reducing the power output.

Conclusions

The 2-D Ritz-Galerkin model is a very useful tool for simulating temperature evolution of PV for different ambient conditions of different geographical locations. It gives transient response of PV with change in irradiance and other weather conditions like ambient temperature, wind speed and sky temperature. It provides spatial distribution of temperature in the cell to find maximum temperature of it. This maximum temperature dictates electrical output of the cell. The simulated PV temperatures are in good agreement with experimental results. We have shown that ambient temperature have considerable effect on the temperature evolution of PV cell and consequently on to its electrical output. Thus performance of cell will vary in different geographical locations and it depends not only on irradiance level but also on ambient temperature.

Acknowledgement

The authors would like to acknowledge the Higher Education Authority through Strand 3 funding, Science Foundation Ireland through their Research Frontiers Program and the Research Support Unit at Dublin Institute of Technology.

Reference

1. Jiang, B., J. Ji, and H. Yi, *The influence of PV coverage ratio on thermal and electrical performance of photovoltaic-Trombe wall.* Renewable Energy, 2008. **33**(11): p. 2491-2498.
2. Radziemska, E., *The effect of temperature on the power drop in crystalline silicon solar cells.* Renewable Energy, 2003. **28**(1): p. 1-12.
3. Chenni, R., et al., *A detailed modeling method for photovoltaic cells.* Energy, 2007. **32**(9): p. 1724-1730.
4. Kim, J.P., et al., *Numerical analysis on the thermal characteristics of photovoltaic module with ambient temperature variation.* Solar Energy Materials and Solar Cells. **95**(1): p. 404-407.
5. J.N.Reddy, D.K.G., *The Finite Element Method in Heat Transfer and Fluid Dynamics*. second ed: CRC 469.
6. J.T.Oden, J.N.R., *Variational Methods in Theoratical Mechanics*. second edition ed. 1983: Springer-Verlag, Berlin.
7. A.F.Mills, *Heat Transfer*. Second ed. 1999: Prentice-Hall, Inc.
8. Churchill, S.W. and H.H.S. Chu, *Correlating equations for laminar and turbulent free convection from a vertical plate.* International Journal of Heat and Mass Transfer, 1975. **18**(11): p. 1323-1329.
9. Bathe, K.-J., *Finite Element Procedures*. 1996: Prentice-Hall, Inc.
10. Meschke, D.K.a.G., *Finite Element Methods in Linear Structural Mechanics*. 2004. 154.
11. Hohmann, P.D.a.A., *Numerische Mathematik I. Eine algorithmisch orientierte Einfuehrung.* 1993: Walter de Gruyter, Berlin.
12. Douglas, C.C., *A User Guide for MADPACKS*. July 1995, Department of Computer Science, Yale University, USA.
13. Rajasankar, J., N.R. Iyer, and T.V.S.R. Appa Rao, *A procedure to assemble only non-zero coefficients of global matrix in finite element analysis.* Computers & Structures, 2000. **77**(5): p. 595-599.
14. Reese, S., *Numerical Methods in Dynamics*. 2003, Lehrstuhl fuer Numerische Mechanik & Simulationtechnik, RUB: Bochum.
15. Rosell, J.I. and M. Ibáñez, *Modelling power output in photovoltaic modules for outdoor operating conditions.* Energy Conversion and Management, 2006. **47**(15-16): p. 2424-2430.